Effectiveness of Distributed Acoustic Sensing for Acquiring Surface Wave Dispersion Data using Multichannel Analysis of Surface Waves

Joseph P. Vantassel[1*[0000-0002-1601-3354]], Brady R. Cox[2[NA]], Peter G. Hubbard[3[0000-0003-3537-8225]], Michael Yust[1[NA]], Farnyuh Menq[1[NA]], Kyle Spikes[1[0000-0002-4732-4657]], and Dante Fratta[4[0000-0003-0478-6760]]

[1] The University of Texas at Austin, Austin TX 78712, USA
[2] Utah State University, Logan UT 84322, USA
[3] University of California Berkeley, Berkeley CA 94720 USA
[4] University of Wisconsin-Madison, Madison WI 53706 USA
*corresponding author: jvantassel@utexas.edu

Abstract. Distributed acoustic sensing (DAS) is a rapidly expanding tool to sense vibrations and system deformations in many engineering applications. In terms of site characterization, DAS presents the ability to make static and dynamic strain measurements on a scale (e.g., kilometers), density (e.g., meter-scale), and fidelity (e.g., microstrain) that was previously unattainable with traditional measurement technologies. In this study, we assess the effectiveness of using DAS to extract surface wave dispersion data using the multichannel analysis of surface waves (MASW) technique. We utilized both highly-controlled, broadband vibroseis shaker truck and more-variable, narrow-band sledgehammer sources to excite the near surface and compared the DAS-derived dispersion data directly with concurrently acquired traditional geophone-derived dispersion data. We report that the differences between the two sensing approaches are minimal and well within the uncertainty bounds associated with each individual measurement for the following DAS testing conditions: (a) a tight-buffered or strain-sensing fiber optic cable is used, (b) the cable is buried in a shallow trench to enhance coupling, and (c) short gauge lengths and small channel separations are used. Our deployed conditions are more promising than previous attempts documented in the literature, thereby demonstrating that DAS can provide accurate measurements of surface wave dispersion data of the same quality as geophones. We show that frequency-dependent normalization of the dispersion image removes the effects of scaling, integration, and differentiation of the measured data, thereby removing the need to post-process the geophone-derived and DAS-derived waveforms into equivalent units before performing dispersion processing. Finally, we summarize the important effect of gauge length on the dispersion data for future reference. This study demonstrates that DAS, when appropriate considerations are made, can be used in-lieu of traditional sensors (i.e., geophones) for making high-quality measurements of surface wave dispersion data using the MASW technique.

Keywords: high density arrays, DAS, geophones, dispersion, surface waves

1 Introduction

Distributed acoustic sensing (DAS) is an emerging technology with broad applications in infrastructure health monitoring and site characterization (Hubbard et al., 2022, 2021; Lindsey et al., 2020; Spikes et al., 2019; Wang et al., 2018). DAS permits the acquisition of static and dynamic signals at scales of tens of kilometers and meter spatial resolutions previously unattainable with traditional sensing technologies (Soga and Luo, 2018). DAS, and for that matter, the larger area of distributed fiber optic sensing (DFOS), requires three main system components: a fiber-optic cable, an interrogator unit (IU), and a dedicated storage, computation, and visualization resource. The fiber-optic cable is the sensing instrument whose elongation or compression (i.e., strain) is measured by the DAS system. Fiber-optic cables are specially designed to propagate the light emitted by the interrogator unit with minimal loss, allowing light to travel (and therefore strain measurements to be made) over large distances (i.e., tens of kilometers) (Lindsey and Martin, 2021). Note that the fiber must be selected and installed carefully to ensure acceptable results; however, as even specially designed fiber-optic cables for strain-sensing applications are relatively inexpensive (between $3 and $7 per meter) they are typically not retrieved for re-use after testing concludes. The second component, the IU, is connected to one end of the fiber-optic cable to send pulses of light down the length of the fiber and measure the returned Rayleigh backscatter events. The IU senses the Rayleigh backscattering caused by imperfections in the silica within the fiber and interprets the phase change as measurements proportional to the local strain along the fiber (Karrenbach et al., 2019). The IU uses precise timing and fast sampling rates (i.e., up to 100s of kHz) to interpret the scattering events as one-dimensional measurements of local strain at various physical distances along the fiber. The dedicated storage, computational, and visualization resource is typically a high-end computer, with large amounts of dedicated storage (at least multiple terabytes), and a real-time data acquisition software interface to facilitate the visualization and interpretation of DAS measurements.

The multichannel analysis of surface waves (MASW) is an active-source surface-wave testing technique for measuring a site's surface wave dispersion from recordings of dynamic signals with strong surface wave content (Park et al., 1999). The MASW technique most commonly involves a linear array of receivers, typically geophones (i.e., velocity transducers), and a surface wave source located collinear with the array and operated by the experimenters. Geophones are most commonly oriented vertically, but they can be oriented horizontally in the in-line or cross-line direction (i.e., sensing particle motion collinear with or perpendicular to the array, respectively). Just as with the geophones, the seismic source may be oriented vertically, horizontally in-line, or horizontally cross-line, depending on the types of surface waves one desires to utilize (Vantassel and Cox, 2022).

In this paper, we examine the fitness of DAS to acquire dynamic strains to extract surface wave dispersion data using MASW. This study compares a 94-m section of a 200-m long strain-sensing fiber-optic cable with an adjacently deployed 94-m long geophone array (48 receivers at a 2-m spacing). The array recorded dynamic signals rich

in surface wave energy generated by off-end vibroseis and impulse sources. The dispersion extracted from both measurement systems shows excellent agreement. This study demonstrates that DAS can be used as a replacement for traditional geophone deployments for extracting surface wave dispersion data.

2 Experimental Setup

This experiment was conducted at the NHERI@UTexas (Stokoe et al., 2020) Hornsby Bend test site in Austin, Texas, USA. Figure 1 shows a plan view of the experimental setup: a 94-m geophone array deployed alongside 200 meters of fiber-optic cable. The DAS array consisted of two fiber-optic cables buried alongside one another, one from NanZee Sensing Technology (NZS-DSS-C02) and the other from AFL (X3004955180H-RD). However, only results from the NanZee cable will be discussed here for brevity. Both cables have tight buffered optical fibers and are constructed such that strain is transferred from the exterior to the core. The AFL cable was designed for tactical telecommunications applications while the NanZee cable was specifically designed for strain sensing (Zhang et al., 2021). Note that the fiber-optic cables are sensitive to strain along their length (i.e., in the horizontal in-line direction). The signals on the two cables were recorded simultaneously by splicing the NanZee and AFL cables together at the far end of the array. On the near-side of the array, the fiber was connected to an OptaSense ODH4 IU, and the other end was appropriately terminated to reduce end reflections. This IU allows for a variable gauge length, we selected the minimum available gauge length of 2.04 m. For those readers who may not be familiar, the gauge length represents the length of fiber that the elongation (or strain) is measured/averaged over at each sensing position. The channel separation, as configured in this study, is the distance between each gauge lengths' centers, and it was set at 1.02 m. The effect of gauge length and channel separation on surface wave dispersion will be discussed later in this work. The IU's sampling frequency (or ping rate) was set at 100 kHz. After acquisition, the purposely over-sampled raw measurements (for the purposes of increasing the acquisition's signal-to-noise and dynamic range) were appropriately downsample to 1 kHz and high-pass filtered at 3 Hz. Immediately adjacent to the fiber-optic cables, two geophone arrays (one vertical and one horizontal in-line) were deployed. However, for brevity, only the results from the horizontal in-line geophones (i.e., those sensing in the same direction as the DAS array) will be discussed in this study. The 48 vertical and 48 horizontal 4.5-Hz Geospace Technologies (GS-11D) geophones were deployed at a constant 2-m spacing. The geophones were mounted in PC21 land cases and coupled to the ground surface with 7.6-cm aluminum spikes. Note that geophone arrays with equal length and channel spacing to the DAS could not be deployed due to equipment constraints. Signals from the geophone arrays were recorded simultaneously at 1 kHz using four interconnected 24-channel Geometric Geode seismographs.

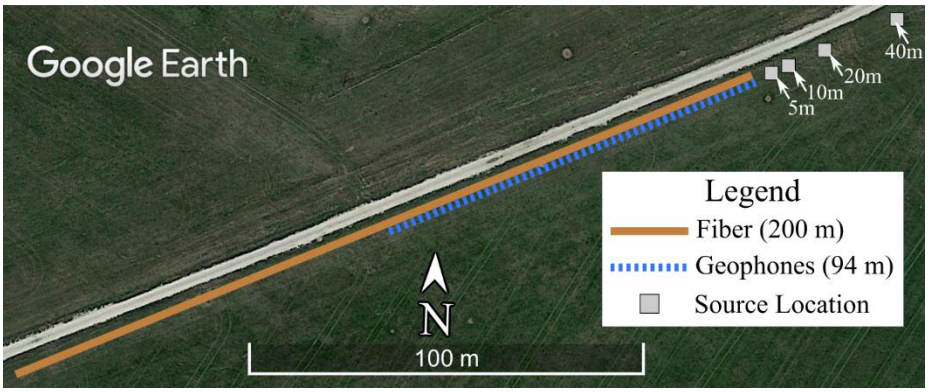

Fig. 1. Plan view of the experimental setup at the Hornsby Bend test site in Austin, Texas, USA, where 200 m of fiber-optic cable was deployed alongside a 94-m long geophone array (48 receivers at a 2 m spacing) to assess the effectiveness of using distributed acoustic sensing (DAS) for recording surface wave propagation. Surface wave energy was produced from four distinct shot locations denoted as 5 m, 10 m, 20 m, and 40 m.

3 Data Acquisition

The DAS and geophone arrays were used to simultaneously record actively generated surface waves using highly controlled vibroseis shaker trucks and more variable sledgehammer impact sources. The vibroseis sources include the specialized three-dimensional shaker T-Rex and the highly-mobile one-dimensional shaker Thumper from the NHERI@UTexas experimental facility (Stokoe et al., 2020). T-Rex was used to shake the ground in all three directions (i.e., vertically, horizontally in-line, and horizontally crossline). However, only the vertical and horizontal in-line shakes are discussed here. T-Rex was used to produce a 12-second chirp with frequencies swept linearly from 3 to 80 Hz. The other vibroseis source Thumper was used to shake vertically following a 12-second chirp with frequencies swept linearly from 5 to 200 Hz. The impact source used for this study was an instrumented 5.4 kg sledgehammer from PCB Piezotronics. The frequency content produced by the sledgehammer is highly variable and depends on the operator and the tested material. All four sources (i.e., T-Rex shaking vertically, T-Rex shaking horizontally in-line, Thumper shaking vertically, and the sledge hammer striking vertically) were deployed in-line at 5, 10, 20, and 40 m away from the start of the DAS fiber-optic cable and geophone array. The source positions relative to the array are shown in Figure 1. Three vibroseis chirps and five sledge hammer impacts were stacked in the time-domain to produce a single vibroseis or sledge hammer waveform at each sensing location with higher signal-to-noise ratio.

4 MASW Processing

Only the first 94 m of the 200-m long DAS array was used during MASW processing to ensure a fair comparison between the geophone-derived and DAS-derived dispersion. All MASW processing was performed using the frequency-domain beamformer with cylindrical-steering vector and square-root weighting (Zywicki and Rix, 2005). A comparison of dispersion images from the geophone array and NanZee cable DAS array is made in Figure 2 for a vertical sledgehammer impact at the 5 m source location. We utilize frequency-dependent normalization of the dispersion image, where we normalize the surface wave energy at each frequency by its maximum, to remove the effects of scaling, integration, and differentiation and thereby allow us to process the geophone-derived and DAS-derived waveforms in their raw units. The small white circles shown in each panel indicate the relative phase velocity maximums selected via an algorithmic relative peak search. From examining Figure 2, we first observe the complexity of the Rayleigh-wave dispersion at the Hornsby Bend site, with the presence of multiple Rayleigh-wave modes. Second, when comparing Figures 2a and 2b, it is clear that the geophone array acquires shorter wavelengths than the DAS array. Specifically, the lower right-hand corner of Figure 2b indicates that the DAS dispersion data for this offset cannot be extracted for wavelengths less than about 2 m indicated by a light-colored dashed line. This observation, which is confirmed by other data acquired at the site (see Figure 3), shows a relationship between the minimum wavelength of surface wave dispersion acquired and the DAS system's gauge length. In particular, there is very limited coherent surface wave energy at wavelengths less than approximately 2 m for the DAS array for any source-offset combination. In contrast, we are able to clearly resolve such wavelengths using the geophone array. This is especially notable given that the DAS data is acquired with a 1.02 m channel separation whereas the geophone data is acquired at a 2 m receiver spacing. This effect shows that when sufficiently small channel separations are used it is the gauge length that controls the shortest wavelength surface waves DAS can measure. While unfortunately there is insufficient room in the current work to fully discuss the physics behind the gauge length's limiting effect, we do note that it is the result of a 180 degree phase shift that occurs for wavelengths between 0.5 and 1 gauge lengths and more generally every $(n+1)^{-1}$ to n^{-1} gauge lengths where n is an odd integer. While this limitation of DAS is not particularly troublesome for the present study, because a short gauge length was able to be used, this observation is critically important for those using DAS systems with much larger minimum gauge lengths. Therefore, when using DAS systems for surface wave acquisition for engineering applications, where short wavelengths are critical for correctly resolving the stiffness of near-surface layers, two factors must be considered. Those two factors are the trace separation, and especially, the gauge length, which must be selected to be sufficiently short to permit good near-surface resolution. The reader will note that the gauge length limitation discussed here for MASW is less restrictive than those proposed by others for other imaging techniques (e.g., Dean et al., 2017) as MASW is primarily sensitive to changes in phase and is not greatly affected by amplitude-related effects provided they are consistent across the array as they are in this case.

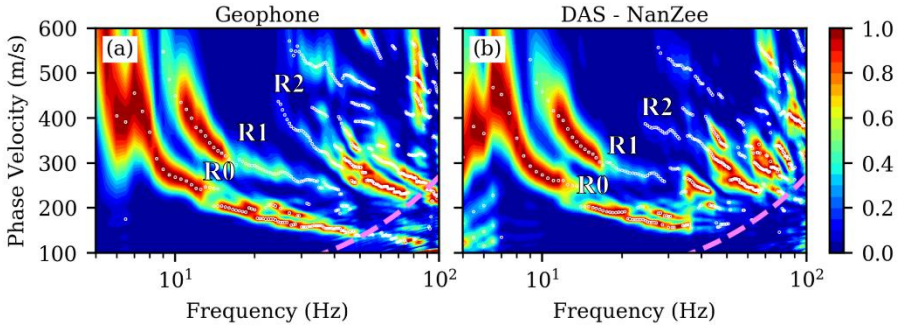

Fig. 2. Comparison of surface wave dispersion images derived from the stacked vertical sledge hammer impacts at a distance of 5 m away from the array as derived from (a) geophone array and (b) NanZee cable of the DAS array. The small white circles shown in each panel indicate the relative phase velocity maximums selected from the dispersion images and later used to identify multiple Rayleigh modes of surface wave propagation. The apparent fundamental, first-higher, and second-higher Rayleigh wave modes are denoted as R0, R1, and R2, respectively. The dashed line in each panel's lower right denotes a wavelength equal to the IU's gauge length (i.e., 2.04 m).

5 Extraction of Experimental Dispersion Data

The frequency-phase velocity peaks from all 16 source-position and source-type combinations were extracted from their respective dispersion images. These peaks were interactively trimmed to isolate three clear Rayleigh modes and summarized into dispersion statistics following the workflow developed by Vantassel and Cox (2022). The interactively-trimmed peaks and dispersion statistics (mean +/- one standard deviation) are shown for the geophone array and NanZee cable of the DAS array in Figure 3a and 3b, respectively. To facilitate a more direct comparison, Figure 4 plots the dispersion statistics from the geophone-derived and DAS-derived experimental dispersion data directly on top of one another. Excellent agreement is observed between the two sensing systems. We note that at high frequencies the consistency between the geophone-derived and DAS-derived dispersion data decreases slightly for the R0 and R1 modes. This slight decrease in consistency is due in part to less clear dispersion trends in these regions (recall Figure 2) that make consistent interactive trimming difficult. Nonetheless, the geophone-derived and DAS-derived experimental dispersion data is in excellent agreement, thereby demonstrating that when appropriate considerations are made (i.e., proper cable selection, good cable-soil coupling, and sufficiently short gauge length and trace separation) DAS can be used to measure surface wave dispersion data that is of equal quality to that acquired using geophones.

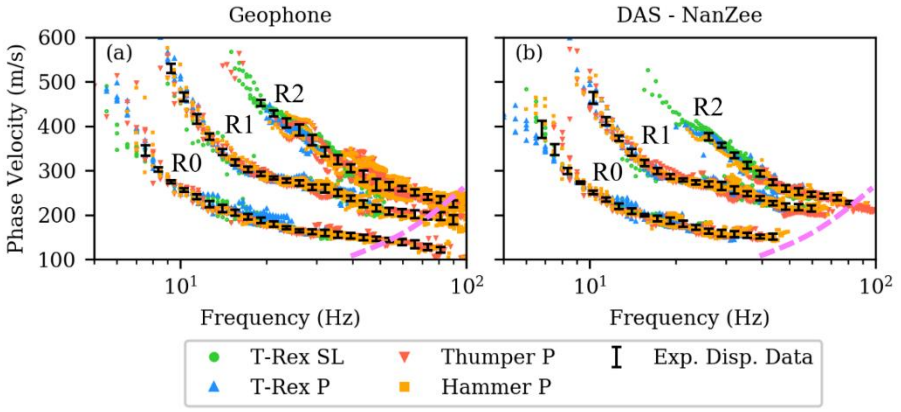

Fig. 3. Experimental dispersion data after performing interactive trimming to isolate the first three Rayleigh modes (i.e., R0, R1, and R2) for the: (a) geophone array, and (b) NanZee cable of the DAS array. The statistical representation of each mode is denoted by error bars that delineate the +/- one standard deviation range. The dashed line in each panel's lower right denotes a wavelength equal to the IU's gauge length (i.e., 2.04 m).

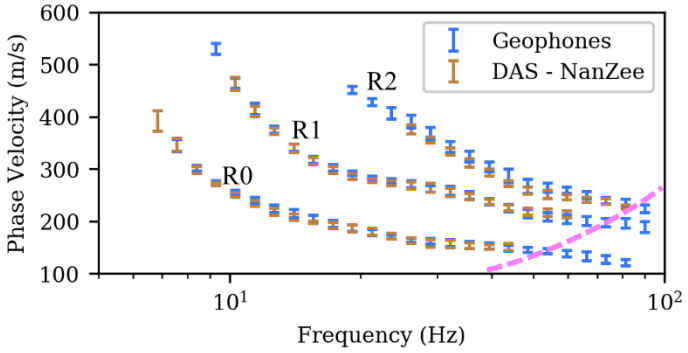

Fig. 4. Comparison between the geophone-derived and DAS-derived experimental dispersion data at the Hornsby Bend test site. The vertical error bars at each frequency represent the mean +/- one standard deviation of the experimental dispersion data for the fundamental, first-higher, and second-higher Rayleigh modes (R0, R1, and R2, respectively). The dashed line to the lower right denotes a wavelength equal to the IU's gauge length (i.e., 2.04 m).

6 Conclusions

We assess the effectiveness of using DAS for extracting dispersion data using the MASW technique. The DAS data from a tightly-buffered, strain-sensing fiber-optic cable buried in a shallow trench were compared with dispersion data extracted from horizontal geophones coupled to the ground surface using an aluminum spike. Wavefields with strong Rayleigh-type surface wave content were generated by using highly-controlled vibroseis sources and more-variable impact sources at four distinct source posi-

tions. The use of frequency-dependent normalization allowed the raw geophone-derived waveforms, proportional to velocity, and the raw DAS-derived waveforms, proportional to strain/displacement, to be used for dispersion processing in their raw units and eliminate the need to convert the measurements into consistent units. Using a relative-peak search three Rayleigh wave modes of propagation were able to be extracted over a relatively broad frequency range for active-source studies (~6 to 70 Hz). A limiting gauge length effect was observed for the DAS-derived dispersion data, where wavelengths shorter than approximately the gauge length could not be resolved despite using a 1.02-m trace separation, thereby making gauge length selection an important factor to consider in future near-surface studies using DAS. The limitation of DAS at short wavelengths aside, the experimental dispersion data recovered from the geophone and DAS systems show excellent agreement for all three recovered Rayleigh modes. Therefore, when appropriate considerations are made to ensure proper cable selection, good cable-soil coupling, and sufficiently short gauge lengths and trace separations, DAS can be an effective alternative to geophones for the purpose of acquiring dynamic signals for the intent of extracting surface wave dispersion data using MASW.

Acknowledgements

This work was supported in part by the U.S. National Science Foundation (NSF) grants CMMI-2037900, CMMI-1520808, and CMMI-1931162. However, any opinions, findings, and conclusions or recommendations expressed in this material are those of the authors and do not necessarily reflect the views of NSF. Special thanks to Dr. Kevin Anderson at Austin Water - Center for Environmental Research for the access to the Hornsby Bend Biosolids Management Plant test site. Special thanks to Dr. Kenichi Soga for the contribution of the NanZee cable used in this study. Special thanks to Todd Bown and the OptaSense team for their assistance in configuring the ODH4, extracting and filtering the DAS-derived seismic waveforms, and permitting us to publish these results. Active-source surface wave processing and calculation of dispersion statistics were performed using the Python package *swprocess* v0.1.0b0 (Vantassel, 2021a). Subsequent operations with the dispersion statistics were performed using the Python package *swprepost* v1.0.0 (Vantassel, 2021b).

References

Dean, T., Cuny, T., Hartog, A.H., 2017. The effect of gauge length on axially incident P-waves measured using fibre optic distributed vibration sensing: Gauge length effect on incident P-waves. Geophysical Prospecting 65, 184–193. https://doi.org/10.1111/1365-2478.12419

Hubbard, P.G., Ou, R., Xu, T., Luo, L., Nonaka, H., Karrenbach, M., Soga, K., 2022. Road Deformation Monitoring and Event Detection using Asphalt-embedded Distributed Acoustic Sensing (DAS). https://doi.org/10.31224/osf.io/mer43

Hubbard, P.G., Xu, J., Zhang, S., Dejong, M., Luo, L., Soga, K., Papa, C., Zulberti, C., Malara, D., Fugazzotto, F., Garcia Lopez, F., Minto, C., 2021. Dynamic structural health monitoring of a model

wind turbine tower using distributed acoustic sensing (DAS). J Civil Struct Health Monit 11, 833–849. https://doi.org/10.1007/s13349-021-00483-y

Karrenbach, M., Cole, S., Ridge, A., Boone, K., Kahn, D., Rich, J., Silver, K., Langton, D., 2019. Fiber-optic distributed acoustic sensing of microseismicity, strain and temperature during hydraulic fracturing. GEOPHYSICS 84, D11–D23. https://doi.org/10.1190/geo2017-0396.1

Lindsey, N.J., Martin, E.R., 2021. Fiber-Optic Seismology. Annu. Rev. Earth Planet. Sci. 49, 309–336. https://doi.org/10.1146/annurev-earth-072420-065213

Lindsey, N.J., Yuan, S., Lellouch, A., Gualtieri, L., Lecocq, T., Biondi, B., 2020. City-Scale Dark Fiber DAS Measurements of Infrastructure Use During the COVID-19 Pandemic. Geophys. Res. Lett. 47. https://doi.org/10.1029/2020GL089931

Park, C.B., Miller, R.D., Xia, J., 1999. Multichannel analysis of surface waves. GEOPHYSICS 64, 800–808. https://doi.org/10.1190/1.1444590

Soga, K., Luo, L., 2018. Distributed fiber optics sensors for civil engineering infrastructure sensing. Journal of Structural Integrity and Maintenance 3, 1–21. https://doi.org/10.1080/24705314.2018.1426138

Spikes, K.T., Tisato, N., Hess, T.E., Holt, J.W., 2019. Comparison of geophone and surface-deployed distributed acoustic sensing seismic data. GEOPHYSICS 84, A25–A29. https://doi.org/10.1190/geo2018-0528.1

Stokoe, K.H., Cox, B.R., Clayton, P.M., Menq, F., 2020. NHERI@UTexas Experimental Facility With Large-Scale Mobile Shakers for Field Studies. Front. Built Environ. 6, 575973. https://doi.org/10.3389/fbuil.2020.575973

Vantassel, J., 2021a. jpvantassel/swprocess: v0.1.0b0. Zenodo. https://doi.org/10.5281/zenodo.4584129

Vantassel, J., 2021b. jpvantassel/swprepost: v1.0.0. Zenodo. https://doi.org/10.5281/zenodo.5646771

Vantassel, J.P., Cox, B.R., 2022. SWprocess: A workflow for developing robust estimates of surface wave dispersion uncertainty. Journal of Seismology Accepted.

Wang, H.F., Zeng, X., Miller, D.E., Fratta, D., Feigl, K.L., Thurber, C.H., Mellors, R.J., 2018. Ground motion response to an ML 4.3 earthquake using co-located distributed acoustic sensing and seismometer arrays. Geophysical Journal International 213, 2020–2036. https://doi.org/10.1093/gji/ggy102

Zhang, C.-C., Shi, B., Zhang, S., Gu, K., Liu, S.-P., Gong, X.-L., Wei, G.-Q., 2021. Microanchored borehole fiber optics allows strain profiling of the shallow subsurface. Sci Rep 11, 9173. https://doi.org/10.1038/s41598-021-88526-8

Zywicki, D.J., Rix, G.J., 2005. Mitigation of Near-Field Effects for Seismic Surface Wave Velocity Estimation with Cylindrical Beamformers. J. Geotech. Geoenviron. Eng. 131, 970–977. https://doi.org/10.1061/(ASCE)1090-0241(2005)131:8(970)